Bull Yamaguchi Med School 52(1-2):1-14, 2005

Advancement of Pulmonary Functional Imaging of Nuclear Medicine, Magnetic Resonance (MR) and Computed Tomography

Kazuyoshi Suga, M.D.

Department of Radiology, Yamaguchi University School of Medicine, 1-1-1, Minami-Kogushi, Ube, Yamaguchi 755-8505, Japan
(Received February 2, 2005)

Abstract This paper describes our challenging for producing pulmonary functional imaging in nuclear medicine, magnetic resonance (MR) and computed tomography fields in our institute of Yamaguchi University School of Medicine. These pulmonary functional imaging include ^{99m}Tc-hexamethyl-propyleneamine (HMPAO) and N-isopropyl-p-^{123}I-iodoamphetamine (IMP) scintigraphies, ^{123}I- metaiodobenzylguanidine (MIBG) scintigraphies, pulmonary ^{133}Xenon gas dynamic SPECT, respiratory-gated or breath-hold ^{99m}Tc-Technegas ventilation/ macroaggregated albumin (MAA) perfusion SPECT, non-contrast ECG-gated perfusion MR imaging and gadolinium-diethylene-triamine pentaacetic acid (Gd-DTPA) aerosol ventilation MR imaging, and pulmonary interstitial (magnetic resonance) MR/computed tomographic (CT) lymphographies. These functional imaging can be expected to contribute to the understanding of functional impairment or treatment strategy in various lung diseases.

Key words: pulmonary function, pulmonary perfusion, computed tomography (CT), magnetic resonance (MR) imaging, single photon emission computed tomography (SPECT)

Introduction

Chest computed tomographic (CT) images provide detailed structural information of the lung, and is useful for the assessment of morphologic changes in various lung diseases. Corresponding detailed information on lung function changes is also of great clinical interest, and various pulmonary functional images have been challenged by many investigators in nuclear medicine, magnetic resonance (MR) and computed tomography fields. This paper describes the recently developed pulmonary functional imaging in our institute of Yamaguchi University School of Medicine. These functional imaging include ^{99m}Tc-hexamethyl-propyleneamine (HMPAO) and N-isopropyl-p-^{123}I-iodoamphetamine(IMP) scintigraphies for sensitive detection of lung injury, ^{123}I-metaiodobenzylguanidine (MIBG) scintigraphies for the assessment of the pulmonary neuroadrenergic system,^{133}Xenon gas dynamic SPECT for qualitative and quantitative assessment of regional ventilation on cross-sectional images, respiratory-gated or breath-hold ^{99m}Tc-Technegas ventilation/ macroaggregated albumin (MAA) perfusion SPECTs for significantly reducing the adverse effects of respiratory motion on traditional non-breathing SPECT images, non-contrast ECG-gated perfusion MR imaging and gadolinium-diethylenetriamine pentaace-

tic acid (Gd-DTPA) aerosol ventilation MR imaging as a non-invasive technique for imaging lung ventilation, pulmonary interstitial (magnetic resonance) MR/computed tomographic (CT) lymphographies for sentinel lymph node mapping and biopsy in patients with lung cancer. These functional imaging modalities can be expected to be widely used as useful adjuncts of morphologic CT images and to contribute to the understanding of functional impairment or treatment strategy in various lung diseases.

Nuclear medicine field

(A) ^{99m}Tc-HMPAO and ^{123}I-IMP scintigraphies

Pulmonary microvascular endothelium of many species takes up and metabolized circulating biogenic amines. We have found that radionuclide-labeled lipophilic amines such as ^{99m}Tc-hexamethylpropyleneamine (HMPAO) and N-isopropyl-p-^{123}I-iodoamphetamine (IMP) could sensitively and abnormally accumulate in the lung injured by chemotheraphy or irradiation, regardless of absence of morphologic abnormalities in X-ray radiograph and CT images.[1-4] These radioactive tracers are considered to be localized in the endothelium, due to altered kinetics or extraction caused by endothelial damage. These tracers are useful for evaluation of pulmonary microvascular endothelial function. The ability of extremely high lung uptake of ^{123}I-IMP in the first circulation can be available for the assessment of microvascular perfusion/function, where ^{99m}Tc-MAA can not reach. ^{123}I-IMP also has been reported to show slow clearance from smoker's and cokain-abused lungs and from lungs of various interstitial diseases.[7] This benefit has been applied to assess the treatment effect of thromboarterectomy for chronic pulmonary thromboembolism, and the results of ^{123}I-IMP scintigraphy were more correlated with clinical improvement than those of ^{99m}Tc-MAA perfusion scan.[3][4] Another noteworthy benefit of IMP is a positive uptake in inflammatory and atelectasis lesions, and negative uptake in malignant tumors (except for melanomas which metabolize biogenic amines).[5][6] ^{99m}Tc-HMPAO scintigraphy has currently been enrolled in the clinical trial in Taiwan, for early detection of endothelial damage in patients with various collagen diseases.[7] Currently, as potential agents protective of endothelium from radicals and lipid peroxides activated by chemical substances and irradiation, nitric monoxide, superoxide dismutase, and catalase have been candidates.[1] When such agents become available for clinical use, these radiolabeled lipophilic amines may be available in assessing the effect of treatment, and will contribute to the scintillating future of pulmonary nuclear medicine.

(B) ^{123}I-MIBG Scintigraphy

^{123}I-metaiodobenzylguanidine (MIBG), a radioiodinated analog of the adrenergic neuron-blocking agent guanethidine, shares the same uptake and metabolic pathways with norepinephrine (NE) in the pulmonary neuroadrenergic system (PNS).[8] This radiotracer may potentially serve as an indicator of PNS function. Our preliminary studies have shown decreased MIBG uptake and faster clearance in the irradiated lung areas (Fig. 1).[9] MIBG uptake is frequently decreased even in the irradiated lungs with relatively preserved perfusion assessed by ^{99m}Tc-MAA SPECT scan. The mechanisms causing the poor MIBG uptake in the irradiated lungs may be partly related to the alterations in microvascular endothelial integrity and function. Including our previous electronmicroscopic study in animals, there are considerable evidences of the initial effects of radiation on the microvascular endothelial cells, accompanied by morphologic and functional alterations.[1][2] Dysfunction or denervation of the involved sympathetic neurons can also be an additional mechanism. Focal ischemia due to pulmonary and/or bronchial arterial microangiopathy associated with radiation also may give damages to the sympathetic neurons, and may partly contribute to the reduction in MIBG uptake. Thus, MIBG may have the potential to be a sensitive marker of irradiation lung injury and may facilitate investigation of damage to irradiated lung independently of lung perfusion.

(C) Dynamic ^{133}Xenon gas SPECT

We have developed pulmonary dynamic ^{133}Xe gas SPECT, which enables to accurately

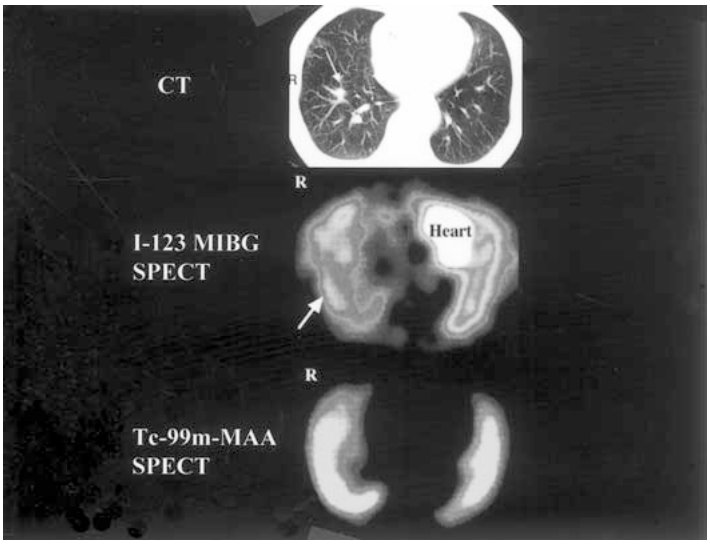

Fig. 1 I-123-MIBG SPECT image in a 68-year-old male with lung cancer who had received 28.5 Gy irradiation to the right lung. Chest CT image shows the irradiated tumor (arrow), without noticeable abnormalities in the surrounding irradiated lungs. I-123-MIBG SPECT image shows a significantly reduced MIBG uptake in the irradiated lung areas, regardless of no significant pulmonary perfusion decrease on ^{99m}Tc-MAA perfusion SPECT image.

evaluate cross-sectional lung function, using a continuous repetitive rotating acquisition mode with a triple-detector SPECT system.[10–12] To eliminate the settling time between projections and acquisition of multiple temporal samples of data, each detector is continuously and repeatedly rotated in the clockwise and counterclockwise directions across the same projection arc. Averaged projection data at the same angle in both directional rotations is used for reconstructing a single SPECT image, so that change in ^{133}Xe activity in the lungs during the acquisition time is averaged. This technique is a useful tool for accurately assessing the extent and location of air trapping in lung regions, without superimposition of lung tissues (Fig. 2). This technique is superior to widely-used planar imaging in the sensitive and accurate detection of ^{133}Xe gas retention in patient's lungs, and is more easily comparable with chest CT images. Regional ventilation abnormality can be quantified by estimating ^{133}Xe half clearance time (T1/2) and mean transit time (MTT) in a pixel basis. We have also developed a topographic three-dimensional image of ^{133}Xe SPECT which simplifies the interpretation of multislice data of ^{133}Xe SPECT and facilitates the perception of anatomic distributions of ^{133}Xe retention sites (Fig. 3).[13–15] This topographic image is also useful for providing the information to non-specialists for nuclear medicine. ^{133}Xe SPECT is especially useful for assessment of regional ventilation abnormality in patients with chronic obstructive pulmonary diseases.[16,17] Using this technique, we demonstrated the difference in the susceptibility of emphysematous changes between peripheral and central lungs and relative preservation of peripheral lung function in smoking-related pulmonary emphysema. We also demonstrated a characteristic feature of periphery-dominant ^{133}Xe retention in patients with diffuse panbronchiolitis.[16] This technique is also useful for evaluating cross-sectional distribution of ^{133}Xe retention associated with bronchial asthma, space-occupying mass lesions such as lung cancer, silicosis, and bronchopulmonary sequestration, and bronchial atresia.[18] This technique already has been introduced in many domestic institutes. The comparison between 3D ^{133}Xe dynamic SPECT images and fast MR imaging which directly visualizes regional respiratory diaphragm/chest wall motions offers investigation of the interaction between impaired

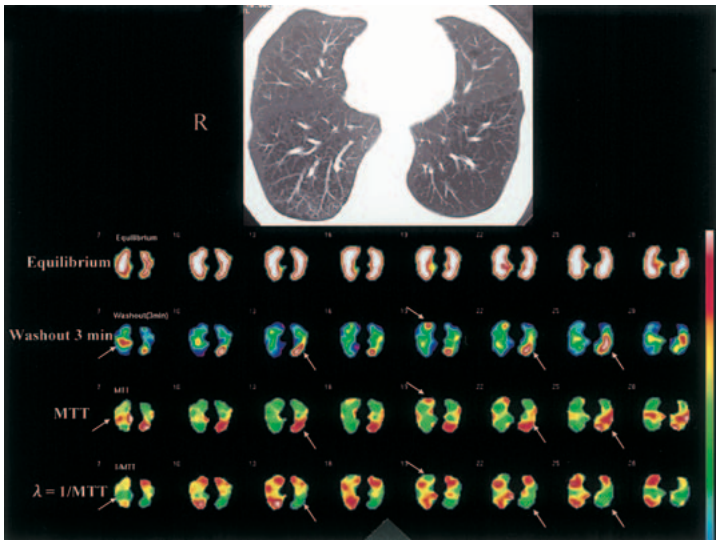

Fig. 2 Dynamic ^{133}Xe gas study in a 68-year-old male with pulmonary emphysema. CT image shows low attenuation areas in both lungs. Transaxial ^{133}Xe dynamic SPECT images show heterogeneous ^{133}Xe gas retention, and prolonged MTTvalues and decreased ventilation rate (λ) in both lungs (arrows). The mean transit time (MTT) values are calculated by a computer for every voxel, based on an area-over-height method; MTT = A . ΔT /H = the total counts collected during washout /the counts at equilibrium, where V is the volume of distribution, F is the air flow (assumed constant), H is the counts during an equilibrium interval of ΔT, and A is the collected counts during washout. λ is a ventilation rate and corresponded to 1/MTT values.

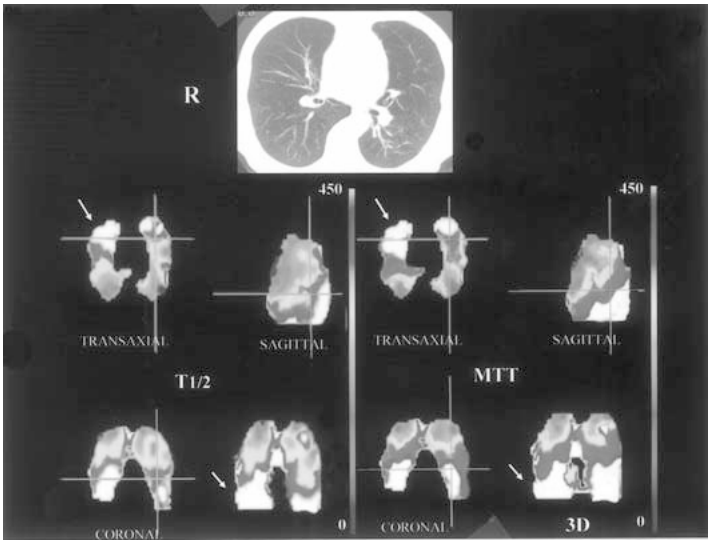

Fig. 3 The 3D functional ^{133}Xe SPECT images in a 69-year-old male with pulmonary emphysema. The volume-rendering 3D functional images and the cross-sectional images at the selected orthogonal lung planes show the heterogeneously prolonged half-clearance time ($T_{½}$) of ^{133}Xe gas washout and MTT values. The worst functioning lung areas are identified in the right lower ventral lungs (arrows).

respiratory mechanics and abnormal lung ventilation in patients with obstructive lung disease.[17]

(D) Respiratory-gated ventilation/perfusion SPECT

In traditional and standard ^{99m}Tc-Technegas ventilation/^{99m}Tc-MAA perfusion SPECT images, respiratory lung motion during image acquisition inherently degrades image sharpness and smear small or ill-defined defects, resulting in underestimation of perfusion impairment/heterogeneity in diseased lungs. To improve this problem, we developed a respiratory-gated SPECT imaging, using a triple-headed SPECT unit and a physiologic respiratory synchronizer, which allows image acquisition only during a specified and brief portion of each respiratory cycle such as end-inspiration or end-expiration (Fig. 4).[19–21] Although the lung count density of the tracer is decreased to approximately one-eighth of that on the conventional SPECT images, the respiratory-gated images could enhance image clarity of perfusion-ventilation defects and sensitively detect functional impairment in various lung diseases (Fig. 5). Furthermore, regional lung radioactivity changes between end-inspiration and end-expiration perfusion SPECT images are expected to uniquely characterize regionally impaired ventilation status.

(E) Breath-hold perfusion SPECT

Another SPECT imaging option to improve adverse respiratory motion effects on traditional ^{99m}Tc-MAA perfusion SPECT is a breath-hold imaging technique. We have recently developed breath-hold SPECT imaging technique, using a continuous rotating acquisition mode of a triple-headed SPECT system and a laser light respiratory tracking device. By monitoring respiratory motion, 20 sec deep-inspiratory breath-hold 360^0 projection data was repeatedly acquired, until 5 adequate data sets with almost the same respiratory dimension could be obtained for reconstructing breath-hold images (Fig. 6). Regardless of decreased lung count density to approximately 25% of conventional images, breath-hold images could provide uniform perfusion in the normal lungs, and enhanced image clarity of perfusion defects in diseased lungs compared with conventional images (Fig. 7). Breath-hold SPECT images can be expected to more sensitively detect impaired perfusion in various lung diseases.

(F) SPECT-CT fusion images

The assessment of functional-morphologic correlation on cross-sectional images is essential for understanding the pathophysiology of diseased lungs. Reliable ventilation-perfusion SPECT-CT fusion images provide detailed function-morphology correlation. However, in the lungs with respiratory motion,

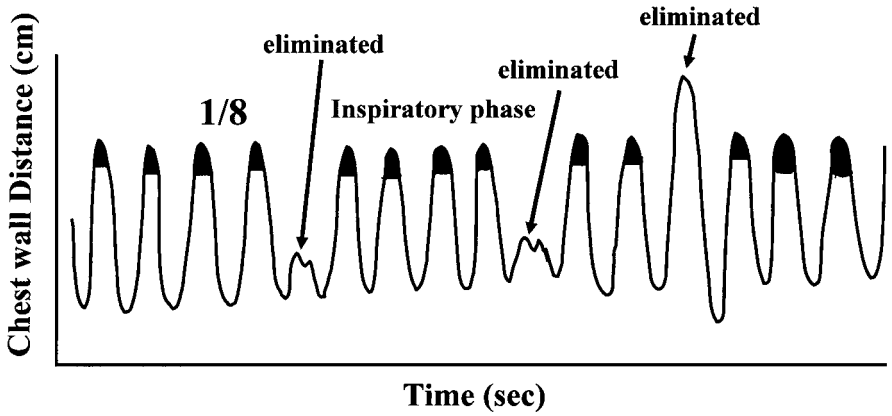

Fig. 4 Schematic presentation of respiratory cycle signals in the physiologic synchronizer. Gated end-inspiration SPECT images are reconstructed from 1/8 threshold data centered at peak inspiration for each regular respiratory cycle (black areas). The data during irregular and inadequate respiratory cycles are automatically eliminated by the computer (arrows).

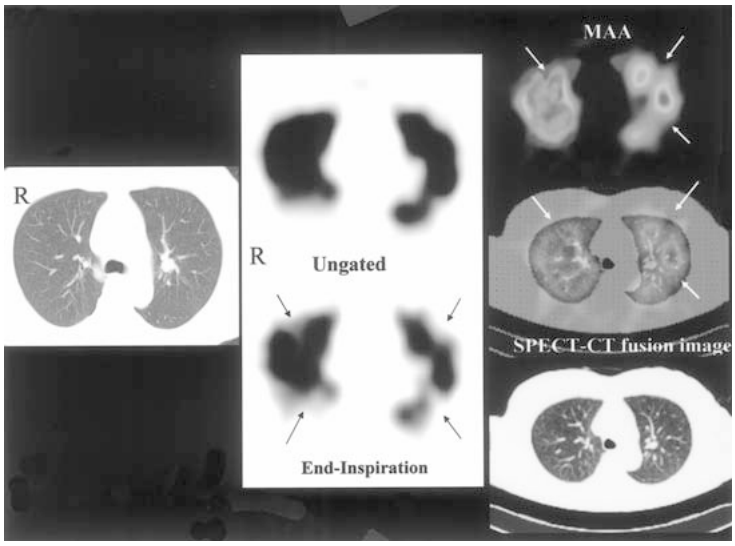

Fig. 5 A-67 year-old female with pulmonary embolism. Chest CT image shows no abnormal opacities in the lung (left). When comparing the ungated and gated end-expiration SPECT images at the CT section level, the segmental and subsegmental perfusion defects are more clearly visualized on the gated image (middle; arrows). The image set of gated perfusion SPECT, co-registered gated perfusion SPET-CT and CT images (transaxial and coronal sections) show the presence of the subsegmental perfusion defects along the corresponding peripheral pulmonary arteries (arrows).

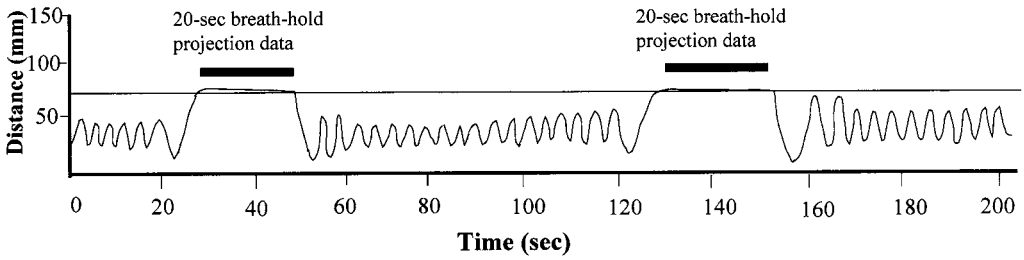

Fig. 6 Schematic presentation of respiratory movement signals on the respiratory monitoring system. Full-inspiratory breath-hold SPECT images are reconstructed from the 5 selected adequate projection data with almost the same respiratory dimension on the respiratory time-distance curves. The remaining breath-hold projection data with inadequate respiratory dimension are eliminated.

there has been a large risk for misregistration between SPECT and CT images. Even though an expensive hybrid CT-SPECT system is recently available, this problem can not be avoided. The respiratory-gated and breath-hold SPECT images described earlier can offer a reliable registration of SPECT and CT images by reducing the risk of misregistration caused by respiratory lung motion.[19)20)] Our preliminary results showed that the gated ^{99m}Tc-MAA perfusion SPECT images yielded a significantly better SPECT-CT match compared with ungated images in 9 round perfusion-defective nodules, (4.9 mm ± 3.1 vs. 19.0 mm ± 9.1; $P < 0.001$). The gated SPECT-CT fusion images allowed accurate perception of the location and extent of each ventilation/perfusion defect on the underlying CT anatomy, and characterized the pathophysiology of the various diseases (Figs.

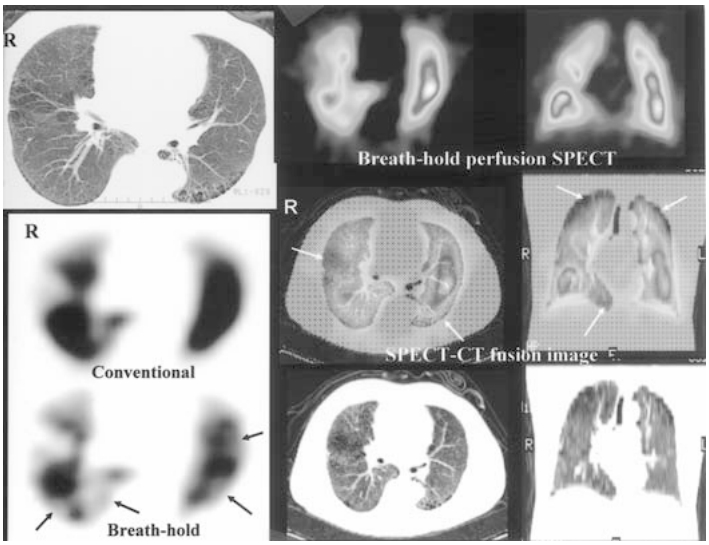

Fig. 7 Fusion images of deep-inspiratory breath-hold perfusion SPECT and CT images in a 64-year-old male with diffuse pulmonary emphysema. Chest CT image (left; top) shows abnormally-low attenuation areas and bullous changes in both lungs. The deep-inspiratory breath-hold perfusion SPECT image at the same CT section level more clearly shows the perfusion defects compared with conventional image (left bottom; arrows). On the image set of transaxial and coronal deep-inspiratory breath-hold SPECT, SPECT-CT fusion and CT images (right), the majority of the perfusion defects are consistent with the low attenuation areas and bullous changes on CT image (arrows), although several defects are seen in the normally-appearing lung areas.

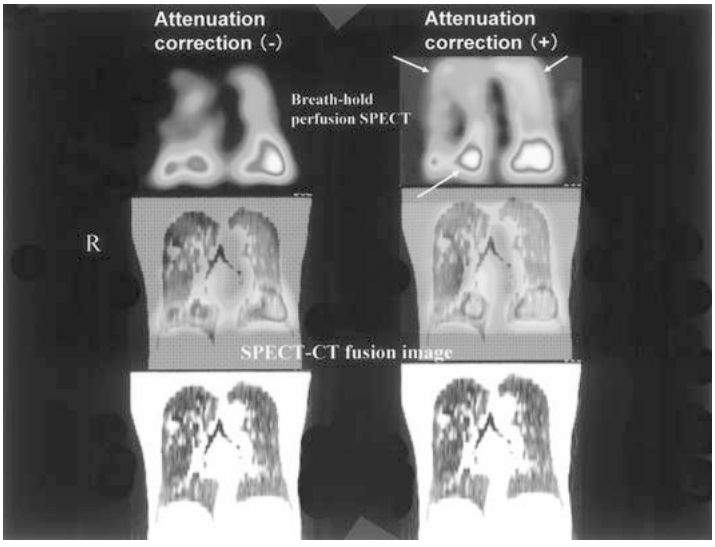

Fig. 8 CT data-based attenuation correction using deep-inspiratory breath-hold SPECT-CT fusion images in a 72-year-old male with lung cancer.The image set of coronal attenuation-corrected/uncorrected SPECT, SPECT-CT fusion and CT images show that pulmonary perfusion is increased especially at deep lung areas near the mediastinum and vertebrae and at the lung apex (arrows).

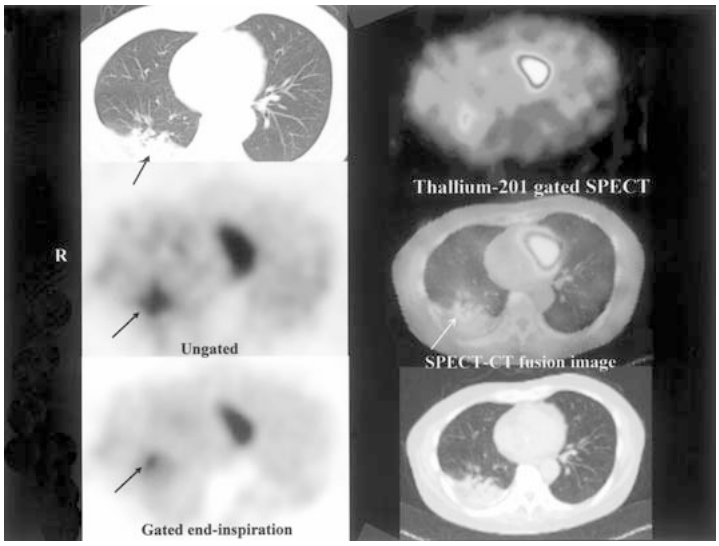

Fig. 9 A 64-year-old male with an endobronchial metastatic tumor and secondary atelectatic changes. Chest CT image (left; top) shows a consolidative opacity in the right lower lobe (arrow). Both of the ungated and gated SPECT images at the corresponding lung level of CT image (left; bottom) show an abnormal ^{201}Tl uptake in the right lower lung, but a focal intensive ^{201}Tl uptake is seen on the gated image, regardless of the surrounding increased ^{201}Tl activity. The image set of transaxial end-inspiratory SPECT, SPECT-CT fusion and CT images (left) confirm that the abnormal ^{201}Tl uptake is located at the proximal bronchi of the consolidative opacity (arrow).

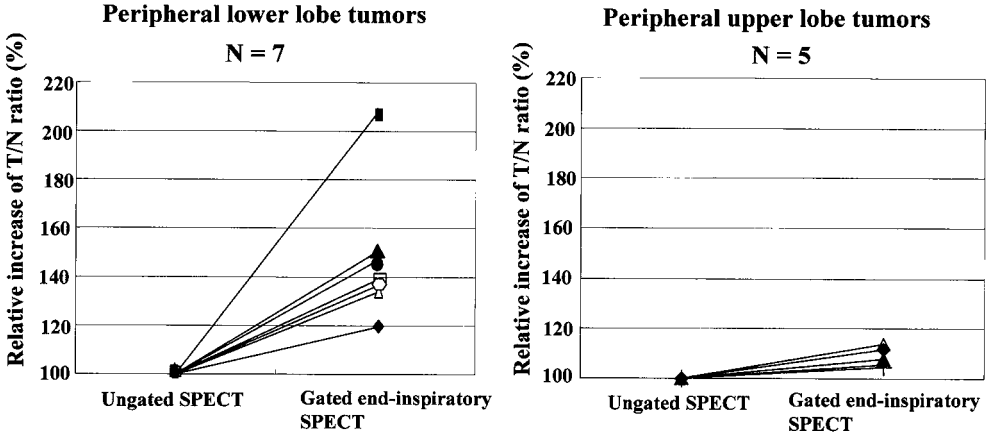

Fig. 10 Comparison of the relative changes in the count ratios of the lesion against the contralateral normal lung area (L/N ratios; calculated by using the mean counts per pixel) of the peripheral lower lobe (left) and upper lobe (right) tumors (L/N ratio in individual tumors on ungated images is normalized as 100%). The same symbol represent the same tumor. Although L/N ratio is increased on gated images compared with that on ungated images in all tumors, the relative increase in L/N ratio of 47.0% ± 28.0 in the 7 lower lobe tumors is significantly higher than that of 8.6% ± 3.8 in the 5 upper lobe tumors ($P < 0.05$).

5, 7). These images also contribute to accurate assessment of regional functional impairment in patients with lung tumors, and appear useful for planning of surgical treatment, prediction of postoperative fun-ction and assessment of external beam radiotherapy effects in patients with lung cancer.[21] Fusion images of respiratory gated/deep-inspiratory breath-hold SPECT and CT images also provide a clinically applicable simple method for CT data-based attenuation correction of ^{99m}Tc-MAA perfusion SPECT images (Fig. 8). The SPECT images are corrected for photon attenuation using attenuation coefficient (μ) maps, which are created from the data of a variable-effective linear μ calculated from spatially-corrected CT data. CT data-based attenuation correction can significantly alter regional perfusion distribution in normal and diseased lungs on perfusion SPECT images, and will permit more accurate assessment of perfusion impairment in various lung diseases.

Respiratory-gated SPECT imaging technique is also applicable for thallium-201 chloride (^{201}Tl) SPECT, and for obtaining reliable fusion images with CT images in patients with malignant lung tumors. In our preliminary study, gated ^{201}Tl SPECT images significantly improved image clarity and contrast of tumor ^{201}Tl uptakes compared with ungated images, regardless of decreased count density due to the use of gated images (Figs. 9, 10).[22] Gated ^{201}Tl SPECT-CT fusion images accurately localize ^{201}Tl uptakes of tumor/lymph node and other focal pathologic/physiologic conditions.

Magnetic resonance (MR) imaging field

(A) Non-contrast ECG-gated lung perfusion images

We have recently developed ECG-gated fast-spin-echo (FSE) MR technique for lung perfusion MR images. This technique enables the image acquisition of the pulsatile lung signal intensity (SI) changes during a cardiac cycle without use of any contrast materials, and a subtraction process between the systolic and diastolic phase images can be expected to provide lung perfusion images.[23–25] In our experimental and clinical studies, the subtracted non-contrast ECG-gated perfusion-weighted images between the systolic and diastolic phase images effectively visualized the perfusion defects in the affected lung areas in both of the airway obstruction and pulmonary embolic subjects (Figs. 11, 12).[26,27]

(B) Gd-DTPA aerosol lung ventilation magnetic resonance (MR) images

Aerosol ventilation study has been performed using technetium-99m-labeled diethylenetriamine pentaacetic acid (^{99m}Tc-DTPA) radioaerosol. However, this method has disadvantages such as, poor spatial resolution, the use of radioactive substances and the difficulties in obtaining cross-sectional tomographic images without overlapping of radioactivity between lesions and normal lungs. To resolve these problems, we have recently developed a gadolinium-DTPA aerosol ventilation MR imaging method.[26,28,29] By using this technique, a sufficient lung aerosol deposition can be noninvasively achieved in the spontaneously breathing animals using an open-circuit aerosol delivery system with an aerosol reservoir. Gd-DTPA aerosol MR images can be simultaneously obtained with the above non-contrast ECG-gated perfusion MR images in the same subject. Our experimental studies showed that these combined MR images effectively defined the matched or mismatched Gd-DTPA aerosol deposition and perfusion defects in the affected areas (Fig. 11).[26]

The measurement of lung clearance of hydrophilic small molecular Gd-DTPA solute (molecular-weight; 742 daltons) deposited in the alveolar space allows the assessment of alveolar transfer changes to small molecular solutes associated with alveolar-capillary membrane damage on cross-sectional imaging. The structural and/or functional damage of the alveolar-capillary membrane in acute lung injury and inflammation induces an increase in the transfer rate of small molecular solutes across this membrane. Our preliminary study using bleomycin (BLM)-injured dog lungs revealed an acceleration of the Gd-AS clearance rate in the acute exudative phase.[29]

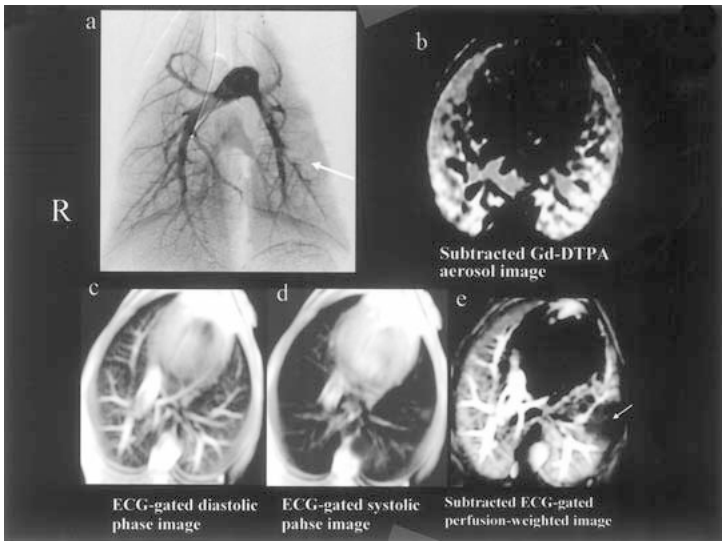

Fig. 11 Pulmonary Gd-DTPA aerosol and non-contrast ECG-gated perfusion MR images in a pulmonary embolic dog. Pulmonary arteriography (a) shows an embolization of the branch of the left lower pulmonary artery with enbucrilate (arrow). The subtracted Gd-DTPA aerosol MR image (b) shows fairly uniform aerosol deposition in both lungs. The subtracted ECG-gated perfusion-weighted image (e) derived from the diastolic and systolic phase images (TReff/TEeff = 919/80 msec) (c, d) shows a perfusion defect in the affected lung area (arrow).

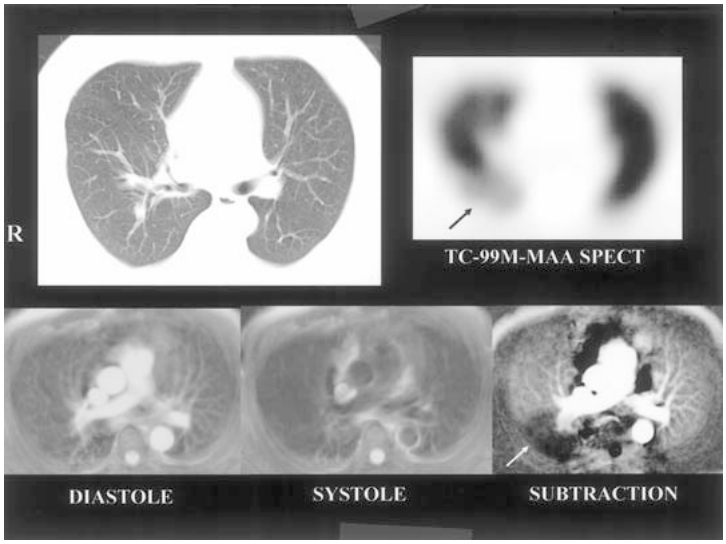

Fig. 12 Pulmonary non-contrast ECG-gated perfusion MR image in a 76-year-old female with pulmonary embolism. Chest CT image does not show noticeable abnormality in the lung (top; left). The subtracted ECG-gated perfusion-weighted MR image (TReff/ TEeff = 560/80 msec) obtained from the diastolic and systolic images shows a perfusion defect in the right dorsal lung (bottom, arrow), which is nearly consistent with that on the matched ^{99m}Tc-MAA SPECT image (top; right, arrow).

(C) Pulmonary magnetic resonance (MR) lymphography

The first lymph node (sentinel lymph node; SLN) encountered by lymphatic vessels draining from malignant tumors appears to reflect the tumor status of the entire lymphatic drainage basin, and is most likely the first to be affected by metastases, and a negative SLN makes it highly unlike that other nodes are affected.[30] Therefore, evaluation of SLN status is critical for minimally invasive surgical treatment in malignant tumors. Recently, several pilot studies of intraoperative lymphoscintigraphic method with the use of radiocolloids and gamma probe have shown the potential feasibility for SLN localization and biopsy in patients with non-small cell lung cancer. However, a scintigraphic method has disadvantages of poor spatial and temporal resolution imaging, which limits its value for accurate identification of the detail of the anatomy of the draining lymphatic basin. Lymphatic connection between the injection site of radiotracer and drainage lymph nodes is barely visualized on scintigrams. Interstitial MR lymphography with intrapulmonary injection of a commercially-available extracellular paramagnetic contrast agent gadopentetate dimeglumine (Gd-DTPA) has the potential utility for imaging pulmonary drainage lymphatic pathways.[30] In our experimental study using dogs, MR lymphography sufficiently visualized the drainage pulmonary lymphatic node station from the injection sites within 5 minutes after intrapulmonary contrast injection in various locations. The location, number and size of the lymph nodes visualized on MR lymphography were consistent with the postmortem anatomy. The extracellular, low molecular-weight agent of Gd-DTPA, which is attached on the alveolar walls, may be easily cleared by lung lymph drainage system, similar to other extracellular, water-soluble, low-molecular solutes, although this contrast agent does not have specific lymphotropic properties.

CT imaging field

Pulmonary CT lymphography

As well as interstitial MR lymphography, interstitial CT lymphography with intrapulmonary injection of a commercially-available, water-soluble extracellular CT contrast agent of iopamidol has the potential utility for imaging pulmonary drainage lymphatic pathways. We have experimentally investigated the utility of this CT lymphography for accurately identifying the lymph nodes directly draining from specific lung portions in dogs, and also have preliminarily used this technique for surgical biopsy of SLN station directly draining from peritumoral lung tissues in patients with operable non-small cell lung cancer.[30,31] CT lymphography clearly visualized the lymph nodes draining from the injection sites in dogs, and all these enhanced nodes could be accurately found at the same locations as actual lymph nodes in the postmortem examination.[30] Although the number of patients with lung cancer was limited, iopamidol could be accurately delivered into peritumoral lung tissues under CT guidance, and all the enhanced lymph nodes on CT lymphography could be accurately found at the pre-operatively identified locations as actual lymph nodes at surgery (Fig. 13).[31] This technique seems to have the potential utility for guiding selective lymph node dissection in minimally invasive surgery for lung cancer.

In conclusion, this paper described our challenging for pulmonary functional imaging in nuclear medicine, MR and CT fields. All these imaging modalities are intended to be non-invasive or minimally-invasive for patients. Although some of these functional imaging modalities are still on an experimental research level, they are expected to be widely used for a routine clinical base in the near future, and contribute to the understanding of lung functional impairment and to minimally-invasive treatment strategy in various lung diseases.

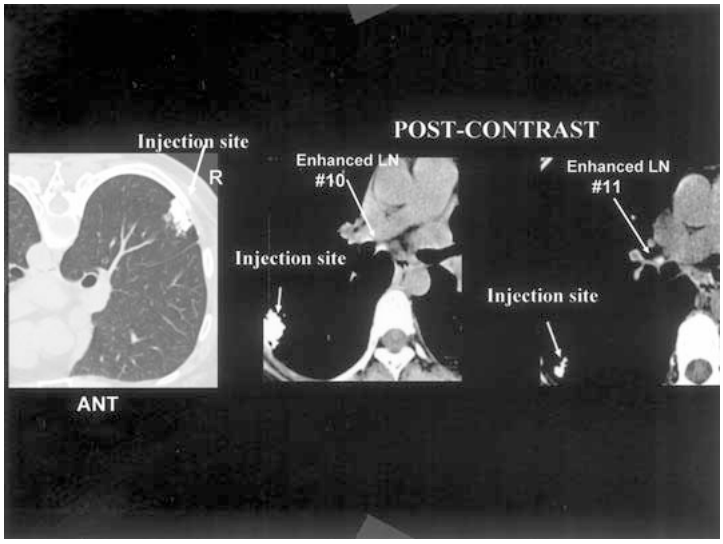

Fig. 13 CT lymphography in a 48-year-old female with lung cancer (adenocarcinoma). Under CT image guideline, iopamidol can be accurately delivered into the peritumoral lung tissue of the right lower lobe (S_6). The ipsilateral hilar lymph nodes of # 11 and #10 are enhanced on post-contrast CT images (left; arrows).

References

1) Suga, K., Uchisako, H., Nishigauchi, K., Shimizu, K., Kume, N., Yamada, N. and Nakanishi, T.: Technetium-99m-HMPAO as a marker of chemical and irradiation lung injury: Experimental and clinical investigations. *J. Nucl. Med.,* **35**: 1520-1527, 1994.

2) Suga, K., Ariyoshi, I., Nakanishi, T., Utsumi, H. and Yamada, N.: Clinical and experimental studies on the mechanism of abnormal accumulation in lung scanning with I-123 IMP. *Nucl. Med. Commun.,* **13**: 282-289, 1992.

3) Suga, K., Ariyoshi, I., Nakanishi, T., Utsumi, H. and Yamada, N.: Altered kinetics of I-123-IMP in irradiated rabbit lungs. *Nucl. Med. Commun.,* **13**: 282-289, 1992.

4) Suga, K., Nishigauchi, K., Sadanaga, M., Kume, N., Uchisako, H., Matsumoto, T. and Nakanishi, T.: I-123 IMP scintigraphy in two patients with primary pulmonary malignant lymphoma. *Ann. Nucl. Med.,* **8**: 65-69, 1994.

5) Suga, K., Nishigauchi, K., Sadanaga, Y., Nishigauchi, K., Uchisako, H. and Nakanishi, T.: Lobar primary pulmonary lymphoma: Iodine-123-iodoam-phetamine and thallium-201 scintigra-phic findings. *J. Nucl. Med.,* **34**: 1980-1983, 1993.

6) Kume, N., Hayashida, K., Cho, I.H., Fukuchi, K., Toba, M., Nakanishi, N., Suga, K. and Matsunaga, N.: Visualization of functional improvement by I-123 IMP lung SPECT after thromboendarterectomy for chronic pulmonary thromboembolism. *Nucl. Med. Commun.,* **20**: 247-253, 1999.

7) Hang, L.W., Hsu, W.H., Tsai, J.J.P., Jim, Y.F., Lin, C.C. and Kao, A.: A pilot trial of quantitative Tc-99m HMPAO and Ga-67 citrate lung scans to detect pulmonary vascular endothelial damage and lung inflammation in patients of collagen vascular diseases with active diffuse infiltrative lung disease. *Rheumatol. Int.,* **24**: 153-156, 2004.

8) Suga, K., Tsukamoto, K., Nishigauchi, K., Kume, N., Matsunaga, N., Hayano, T. and Iwami, T.: Iodine-123-MIBG imaging in pheochromocytoma with cardiomyopathy and pulmonary edema. *J. Nucl. Med.,* **37**: 1361-1364, 1996.

9) Suga, K., Kume, N., Nishigauchi, K., Shimizu, K. and Matsunaga, N.: Potential of I-123-MIBG SPET to detect ab-

normal function status of pulmonary neuroadrenergic system in irradiated lung. *Eur. J. Nucl. Med. Mol. Imaging,* **26** : 647-654, 1999.
10) Suga, K., Nishigauchi, K., Kume, N., Koike, S., Takano, K., Tokuda, O., Matsumoto, T. and Matsunaga, N.: Dynamic pulmonary SPECT of Xenon-133 gas washout. *J. Nucl. Med.,* **37** : 807-814, 1996.
11) Suga, K., Nishigauchi, K., Kume, N., Takano, K. and Matsunaga, N.: Regional ventilatory evaluation using dynamic imaging of Xenon-133 washout in obstructive lung disease; an initial study. *Eur. J. Nucl. Med.,* **22** : 220-226, 1995.
12) Suga, K., Nishigauchi, K., Kume, N., Takano, K., Koike, S., Shimizu, K. and Matsunaga, N.: Ventilation abnormalities in obstructive airways disorder; detection with pulmonary dynamic densitometry by means of spiral CT versus dynamic Xe-133 SPECT. *Radiology,* **202** : 855-862, 1997.
13) Suga, K., Nishigauchi, K., Matsunaga, N., Kawakami, Y., Kume, N., Sugi, K. and Esato, K.: Three-dimensional surface display of dynamic pulmonary xenon-133 SPECT in patients with obstructive lung disease. *J. Nucl. Med.,* **39** : 889-893, 1998.
14) Suga, K., Nishigauchi, K., Matsunaga, N., Shimizu, K., Kume, N., Sugi, K. and Esato, K.: Preliminary application of three dimensional displays of dynamic pulmonary Xenon-133 SPECT in the evaluation of patients with pulmonary emphysema for thoracoscopic lung volume reduction surgery. *Eur. J. Nucl. Med.,* **25** : 410-416, 1998.
15) Suga, K.: Technical and analytic advances in pulmonary ventilation SPECT with xenon-133 gas and Tc-99m-Technegas. *Ann. Nucl. Med.,* **16** : 303-310, 2002.
16) Suga, K., Kume, N., Matsunaga, N., Ogasawara, N., Motoyama, K., Hara, A., Matsumoto, T. : Relative preservation of peripheral lung function in smoking-related pulmonary emphysema: Assessment with Tc-99m-MAA perfusion and dynamic Xe-133 SPET. *Eur. J. Nucl. Med. Mol. Imaging,* **27** : 800-806, 2000.
17) Suga, K., Tsukuda, T., Awaya, H., Matsunaga, N., Sugi, K. and Esato, K.: Interactions of regional respiratory mechanics and pulmonary ventilatory impairment in pulmonary emphysema: Assessment with dynamic MRI and Xenon-133 SPECT. *Chest,* **117** : 1646- 1655, 2000.
18) Suga, K., Hara, A., Maysumoto, T. and Matsunaga, N.: Case report: Intralobar bronchopulmonary sequestration; evidence of air trapping shown by dynamic xenon-133 SPECT. *Br. J. Radiol.,* **74** : 657-661, 2001.
19) Suga, K., Kawakami, Y., Zaki, M., Yamashita, T., Matsumoto, T. and Matsunaga, N.: Pulmonary perfusion assessment with respiratory-gated Tc-99m-MAA SPECT; preliminary results. *Nucl. Med. Commun.,* **25** : 183- 193, 2004.
20) Suga, K., Kawakami, Y., Zaki, M., Ymashita, T., Seto, A., Matsumoto, T. and Matsunaga, N.: Assessment of regional lung functional impairment with co-registered respiratory-gated ventilation/perfusion SPET-CT images: Initial experiences. *Eur. J. Nucl. Med. Mol. Imaging,* **31** : 240-249, 2004.
21) Suga, K., Kawakami, Y., Zaki, M., Yamashita, T., Shimizu, K. and Matsunaga, N.: Clinical utility of co-registered respiratory-gated ^{99m}Tc-Technegas/ MAA SPECT-CT images in the assessment of regional lung functional impairment in patients with lung cancer. *Eur. J. Nucl. Med. Mol. Imaging,* **31** : 1280-1290, 2004.
22) Suga, K., Kawakami, Y., Zaki, M., Yamashita, T., Shimizu, K. and Matsunaga, N.: Initial application of respiratory-gated thallium-201 SPECT in pulmonary malignant tumors. *Nucl. Med. Commun.,* **26** : 303-313, 2005.
23) Suga, K., Ogasawara, N., Okada, M., Tsukuda, T., Mtsunaga, N. and Miyazaki, M.: Definition of lung perfusion impairments in pulmonary embolic and airway obstruction dog models with non-contrast ECG-Gated pulmonary perfusion MR imaging. *J. Appl. Physiol.,* **92** : 2439-2451, 2002.
24) Suga, K., Ogasawara, N., Okada, M. and Matsunaga, N.: Potential of non-contrast ECG-gated fast-spin-echo MR imaging to

monitor dynamically altered perfusion in regional lung. *Invest. Radiol.,* **37** : 615-625, 2003.
25) Suga, K., Ogasawara, N., Okada, M., Matsunaga, N. and Arai, M.: Regional lung functional impairment in acute airway obstruction and pulmonary embolic dog models assessed with gadolinium-based aerosol ventilation and perfusion magnetic resonance imaging. *Invest. Radiol.,* **37** : 281-291, 2002.
26) Ogasawara, N., Suga, K., Kawakami, K., Yamashita, T., Zaki, M. and Matsunaga, N.: Assessment of regional lung function impairment in airway obstruction and pulmonary embolic dogs with combined non-contrast ECG-gated perfusion and Gd-DTPA aerosol MR images. *J. Magn. Reson. Imaging,* **20** : 46-55, 2004.
27) Ogasawara, N., Suga, K., Zaki, M., Okada, M., Kawakami, Y. and Matsunaga, N.: Assessment of lung perfusion impairment in patients with pulmonary artery-occlusive and chronic obstructive pulmonary diseases with non-contrast ECG-gated fast-spin-echo perfusion MR imaging. *J. Magn. Reson. Imaging,* **20** : 601-611, 2004.
28) Suga, K., Ogasawara, N., Okada, M., Tsukuda, T. and Mtsunaga, N.: Assessment of regional lung ventilation in dog lungs with Gd-DTPA aerosol ventilation MR images. *Acta Radiologica,* **43** : 282-291, 2002.
29) Suga, K., Yuan, Y., Ogasawara, N., Tsukuda, T. and Matsunaga, N.: Altered clearance of gadolinium-DTPA aerosol from bleomycin-injured dog lungs; initial observations. *Am. J. Respir. Crit. Care. Med.,* **167** : 1704- 1710, 2003.
30) Suga, K., Yuan, Y., Ogasawara, N., Okada, M., Kawakami, Y. and Matsunaga, N.: Potential of magnetic resonance lymphography with intrapulmonary injection of gadopentetate dimeglumine for visualization of the pulmonary lymphatic basin in dogs: Preliminary results. *Invest. Radiol.,* **38** : 679-689, 2003.
31) Ueda, K., Suga, K., Kaneda, Y., Li, S.T.H., Ueda, K., Hamano, K.: Preoperative Imaging of the lung sentinel lymphatic basin with computed tomographic lymphography: A preliminary study. *Annals. Thorac. Surg.,* **77** : 1033-1038, 2004.